



HAL
open science

PIPERADE: A double Penning trap for mass separation and mass spectrometry at DESIR/SPIRAL2

P. Ascher, L. Daudin, M. Flayol, M. Gerbaux, S. Grévy, M. Hukkanen, A. Husson, A. de Roubin, P. Alfaut, B. Blank, et al.

► To cite this version:

P. Ascher, L. Daudin, M. Flayol, M. Gerbaux, S. Grévy, et al.. PIPERADE: A double Penning trap for mass separation and mass spectrometry at DESIR/SPIRAL2. Nucl.Instrum.Meth.A, 2021, 1019, pp.165857. 10.1016/j.nima.2021.165857. hal-03390279

HAL Id: hal-03390279

<https://hal.science/hal-03390279>

Submitted on 16 Oct 2023

HAL is a multi-disciplinary open access archive for the deposit and dissemination of scientific research documents, whether they are published or not. The documents may come from teaching and research institutions in France or abroad, or from public or private research centers.

L'archive ouverte pluridisciplinaire **HAL**, est destinée au dépôt et à la diffusion de documents scientifiques de niveau recherche, publiés ou non, émanant des établissements d'enseignement et de recherche français ou étrangers, des laboratoires publics ou privés.



Distributed under a Creative Commons Attribution - NonCommercial 4.0 International License

PIPERADE: A double Penning trap for mass separation and mass spectrometry at DESIR/SPIRAL2

P. Ascher^{a,*}, L. Daudin^a, M. Flayol^a, M. Gerbaux^a, S. Grévy^a, M. Hukkanen^{a,b}, A. Husson^a, A. de Roubin^a, P. Alfaut^a, B. Blank^a, K. Blaum^c, B. Lachacinski^a, D. Lunney^d, E. Minaya Ramirez^d, S. Naimi^e, S. Perard^a and B. Thomas^a

^aUniversité de Bordeaux, CNRS/IN2P3, CENBG, UMR5797, 33175 Gradignan, France

^bUniversity of Jyväskylä, P.O. Box 35, FI-40014 Jyväskylä, Finland

^cMax-Planck-Institut für Kernphysik, Saupfercheckweg 1, 69117 Heidelberg, Germany

^dUniversité Paris-Saclay, CNRS/IN2P3, IJCLab, 91405 Orsay, France

^eRIKEN Nishina Center, Wako, Saitama 351-0198, Japan

ARTICLE INFO

Keywords:
Penning trap
DESIR/SPIRAL2
Beam purification
Mass spectrometry

ABSTRACT

A double Penning trap is being commissioned at CENBG Bordeaux for the future DESIR/SPIRAL2 facility of GANIL. The setup is designed to perform both high-resolution mass separation of the ion beam for trap-assisted spectroscopy, and high-accuracy mass spectrometry of short-lived nuclides. In this paper, the technical details of the new device are described. First offline tests with the purification trap are also presented, showing a mass resolving power of about 10^5 .

1. Introduction


The use of ion traps in radioactive ion beam (RIB) facilities has become essential these last decades [1, 2], both for beam quality/purity improvement and for high-accuracy mass spectrometry. After the pioneering ISOLTRAP experiment at ISOLDE/CERN [3], Penning traps have been implemented in various facilities, such as JYFLTRAP/IGISOL [4], LEBIT/MSU [5], TITAN/TRIUMF [6], SHIPTRAP/GSI [7], CPT/CARIBU [8] and TRIGA-TRAP/TRIGA [9], all of them showing that this technique, widely used in other fields (atomic physics, quantum computing, ...), is also extremely powerful in terms of nuclear mass precision, accuracy, sensitivity, efficiency as well as ion manipulation for high-resolution beam purification.

In this context, a double Penning trap named PIPERADE (Pièges de Penning pour les Radionucléides à DESIR, i.e. Penning traps for radionuclides at DESIR) [10, 11] is being developed at Centre d'Etudes Nucléaires de Bordeaux-Gradignan (CENBG) for the future DESIR/SPIRAL2 facility [12, 13] of GANIL. DESIR will be dedicated to low-energy studies through precision measurements of nuclear ground and excited state properties. Decay spectroscopy, laser spectroscopy and trap-based devices will benefit from new 10-60 keV exotic ion beams from: (i) the upgraded SPIRAL1 facility [14], producing light nuclei by ISOL-fragmentation and (ii) the super separator spectrometer S3 [15] under commissioning, producing a wide range of neutron-deficient nuclei (including the refractory elements) by in-flight fusion-evaporation with unprecedented intensities. A second phase may well emerge in the SPIRAL2 project, providing the accessibility to very neutron-rich nuclei by fission reactions.

DESIR will thus be unique in terms of beam intensities. While the production rate is crucial to study exotic nuclei, beam purity is also critically important. Isobaric contamination from non-selective ion production and/or ionization, as well as chemical reactions producing molecular contaminants, are often present with much higher intensities than the ions of interest, preventing certain types of measurements.

Beam purification can be performed using a magnetic dipole separator, such as the DESIR-HRS [16] developed at CENBG for DESIR. It has the advantage to be extremely fast (in-flight separation, i.e. a few tens of μ s), to be able to handle high-intensity beams and it aims to push the current mass resolution limits of such a system, up to 2×10^4 .

*Corresponding author

 ascher@cenbg.in2p3.fr (P. Ascher)

ORCID(s): 0000-0002-1990-0848 (P. Ascher)

46 Nevertheless, even a higher resolution is required to separate a few ions of interest from a large number of con-
 47 taminants, and more generally to separate very close isobars or even long-lived isomers. Indeed, high-precision mea-
 48 surements can be achieved only if the beam is isobarically-pure but also isomerically-pure. Penning traps are known
 49 to reach the highest resolving power, from 10^5 to 10^7 depending on the separation techniques, such as the standard
 50 sideband buffer gas cooling [17], Ramsey cleaning [18, 19] or phase splitting [20, 21, 22]. All these techniques will be
 51 presented in this paper. However, the high-resolution performances of the Penning trap technique come at the price of
 52 long separation times (> 100 ms) and limited numbers of ions, up to 10^2 - 10^3 ions per bunch for the buffer gas cooling
 53 technique and only a few ions per bunch for the other methods. This is a consequence of space-charge effects which
 54 decrease the resolution and the efficiency for larger number of ions [23]. In order to push the limitations of existing
 55 devices further, the first trap of the double Penning trap PIPERADE will be a new type of high-capacity large trap
 56 that aims to separate up to 10^4 - 10^5 ions per bunch using the buffer gas cooling technique. In addition, other cleaning
 57 techniques allowing to reach the highest resolution, and requiring a gas-free trap, will be implemented in the second
 58 trap.

59 The pure beams extracted from the device will be re-injected in the main DESIR beam line, so that various ex-
 60 perimental setups, such as total absorption spectrometry, collinear laser spectroscopy and decay measurements, will
 61 benefit from the trap performances.

62 Besides purification purposes, PIPERADE will be used as a mass-measurement setup on its own. The mass of
 63 an atomic nucleus is one of its most fundamental properties and is therefore a key observable to guide and constrain
 64 the current theoretical descriptions of the nucleus and the nucleon-nucleon interaction. Binding energy measurements
 65 along isotopic chains reveal structure effects [24], such as shell closures [25, 26] or onsets of deformation [27]. In
 66 addition to fundamental nuclear physics questions, experimental masses are crucial to constrain nucleosynthesis mod-
 67 els [28, 29] (rp-process and r-process) and precise Q -value measurements of specific beta transitions have different
 68 applications, as tests of the weak interaction in the Standard Model [30] or the search of candidates for the neutrino
 69 mass measurement [31].

70 In this paper, details on the Penning trap technique will be given, followed by a full technical description of the
 71 PIPERADE system. The setup being now fully in operation, the tests with offline beam are ongoing ; first results using
 72 the first trap will briefly be presented whereas a detailed description of the offline studies will be given in another
 73 publication, in preparation.

74 2. Basics of Penning traps and operational modes of PIPERADE

75 2.1. Principle of a Penning trap and excitation techniques

76 A Penning trap allows the storage of charged particles thanks to the combination of a strong homogeneous magnetic
 77 field for the radial confinement and a static quadrupole electric field for the axial confinement. The electric potential
 78 is obtained by applying a voltage difference U_0 between a central ring electrode and two so-called endcap electrodes
 79 and can be expressed as

$$V(z, \rho) = \frac{U_0}{d^2}(2z^2 - \rho^2) \quad (1)$$

80 where z is the distance along the trap axis from the trap center, ρ the radial coordinate, and $d = \sqrt{z_0^2 + r_0^2/2}$ the
 81 characteristic trap geometry parameter, with z_0 the distance between the ring center and the endcaps, and r_0 the inner
 82 trap radius. The repulsive character of this electric field in the radial direction is compensated by the strong magnetic
 83 field obtained by installing the Penning trap in a superconducting magnet. For creating this quadrupole electric field,
 84 electrodes can be shaped as hyperboloids of revolution. An alternate way is to use a cylindrical trap and by choosing
 85 the potentials and lengths of the electrodes appropriately [32], the electric field can be made very close to a pure
 86 quadrupolar one near the trap center. It is the case of the PIPERADE traps, which are shown in Figure 1.a).

87 The resulting ion motion in a Penning trap is a superposition of three eigenmotions: (i) an harmonic axial motion
 88 along the trap axis at the frequency ν_z , (ii) a modified cyclotron motion at the frequency ν_+ , and (iii) a magnetron motion
 89 at the frequency ν_- . The two latter motions are in the radial plane, the slow magnetron motion is centered at the trap
 90 axis and its orbit defines the center of the modified cyclotron motion. The true cyclotron frequency $\nu_c = qB/2\pi m$,
 91 with q the ion charge, m the ion mass and B the strength of the magnetic field, corresponds, for an ideal trap, to the
 92 sum of the two radial frequencies.

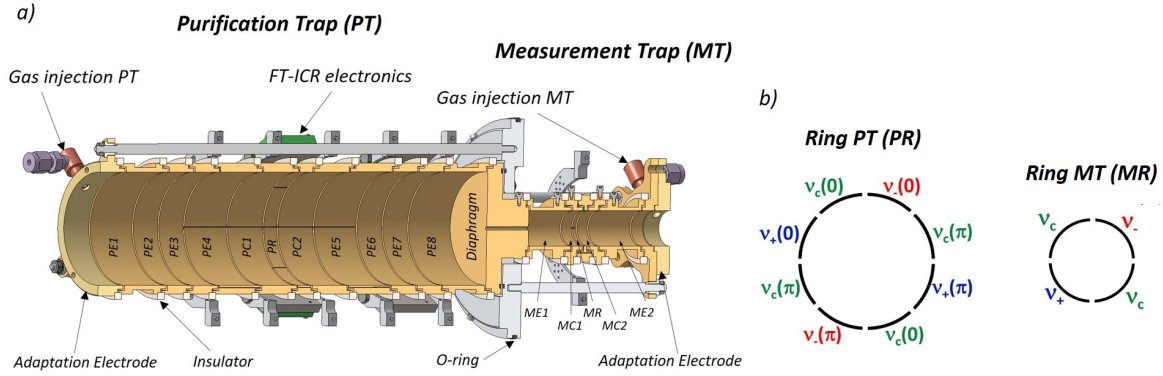


Figure 1: a) The two Penning traps of PIPERADE separated by a diaphragm. The purification trap (PT) consists of eleven electrodes, i.e. two endcap electrodes, which are four-fold axially-segmented (PE1-PE4, PE5-PE8), two correction electrodes (PC1, PC2) and one central ring electrode (PR). The measurement trap (MT) consists of five electrodes, i.e. two endcap electrodes (ME1, ME2), two correction electrodes (MC1, MC2) and one central ring electrode (MR). The electronics for broad-band FT-ICR detection can be seen on top of the purification trap. Gas inlets for helium feedings are fixed on the adaptation electrodes on the far sides of the purification and measurement traps. Dipolar excitation at ν_- is shown in red, dipolar excitation at ν_+ is shown in blue, whereas quadrupolar excitation at ν_c is shown in green.

93 The main interest of a Penning trap lies in the manipulation of these ion motions. Each motion has its own fixed
 94 frequency, defined by the electric and magnetic fields and the charge-to-mass ratio q/m of the trapped ions. However,
 95 the amplitude of these motions can be modified by bringing/removing energy to/from the motions. There are different
 96 ways of doing so, one being to fill the trap with a buffer gas. The ion collisions with the gas atoms will lead to a fast
 97 decrease of the amplitude of both the axial and the modified cyclotron motions, whereas the magnetron motion radius
 98 will slowly increase.

99 The second powerful way to manipulate the ions is to apply radio-frequency (RF) fields on the trap electrodes.
 100 Excitations of the axial motion can be performed by applying RF fields on the endcaps, but in the following only radial
 101 motion excitations will be described. For this, the central ring electrode is used and has to be segmented. In the case
 102 of PIPERADE, as can be seen in Figure 1.b), the ring electrode of the first trap, called the purification trap (PT), is 8-
 103 fold segmented whereas the ring electrode of the second trap, called the measurement trap (MT), is 4-fold segmented.
 104 There are two main modes for performing excitations: the dipolar and the quadrupolar modes.

105 The dipolar mode consists of applying an RF field in one radial direction. If the RF signal is applied at one of
 106 the eigenfrequencies, the radius of the corresponding motion will be modified without changing the others. When the
 107 excitation and the ion motion are in phase, the ions will be pushed from the electrode where the RF signal is applied
 108 every time it passes in front of it, and therefore the radius will increase. Figure 1.b) shows how the two different dipolar
 109 excitations at ν_- or ν_+ are applied on the ring segments. One should note that each trap segment is connected to a
 110 given function generator providing a specific frequency and phase. For the purification trap, opposite phases 0 and π
 111 are applied on opposite segments whereas for the measurement trap, only one phase is applied on a single segment,
 112 also creating a dipolar field component but with lower amplitude.

113 The quadrupolar mode consists of applying an RF signal with the same phase on two opposite segments (see ν_c
 114 excitation in Figure 1.b). For the purification trap, the same RF signal with the opposite phase is additionally applied
 115 to the two other orthogonal segments for a higher quadrupolar field component. This type of field is applied only on
 116 sums of eigenfrequencies and allows to couple motions. A quadrupolar RF excitation at $\nu_c = \nu_+ + \nu_-$ will couple the
 117 modified cyclotron motion to the magnetron motion, i.e. as long as the excitation is applied there will be a periodic
 118 conversion between the amplitudes of both motions. Therefore, what is called a π -pulse excitation corresponds to a
 119 single conversion from a pure motion to another pure one. The period of the interconversion process depends on the
 120 amplitude of the excitation field. An alternate way to couple the radial motions is to use an octupolar mode, which
 121 increases the resolving power [33]. This is technically achieved by using an 8-segmented ring like the purification trap
 122 and by applying the same phase on the four opposite segments at the frequency $2\nu_c$.

123 These dipolar and quadrupolar fields are usually applied by one RF pulse at a given amplitude and for a given
124 duration, which will be inversely proportional to the frequency width of the excitation. Therefore the longer the
125 excitation, the higher the resolution. An alternate way is to use time-separated oscillatory fields, called Ramsey fields
126 [18, 34], by applying two identical pulses separated by a certain time duration, which increases the resolution and the
127 precision of the technique, as it will be explained in the next Section.

128 2.2. Mass separation and mass spectrometry techniques

129 All the various mass separation and mass measurement techniques that will be used at PIPERADE will be based on
130 the above-described manipulation methods. The double-Penning trap PIPERADE device consists of two cylindrical
131 traps, separated by a diaphragm for selection purposes but also to act as a pumping barrier. Indeed, depending on
132 the operational mode the pressure in both traps will have to be different. These different techniques and the main
133 operational modes of PIPERADE are described in the following.

134 2.2.1. PIPERADE as a mass separator

135 PIPERADE will be used for mass separation and will deliver pure beams to the DESIR users for post-trap spec-
136 troscopy. The standard separation technique, which will be used in the purification trap of PIPERADE is the so-called
137 sideband buffer gas cooling technique [17]. It consists of two main steps: first a dipolar excitation is applied at the
138 magnetron frequency ν_- . This frequency being in first-order mass-independent, it results in an increased magnetron
139 radius for all ion species in the trap. The second step uses the combination of a quadrupolar field at ν_c , which converts
140 the magnetron motion into a modified cyclotron motion, and the effect of the buffer gas, which cools the modified
141 cyclotron motion. As the quadrupolar excitation is highly selective, only the ions of interest are re-centered in the trap.
142 By ejecting the ions through the diaphragm, only the re-centered ones are transferred to the measurement trap. This
143 powerful technique has the advantage of removing multiple contaminants, even unidentified ones, to handle large ion
144 bunches (up to 10^2 - 10^3 ions) and to reach resolutions up to 10^5 . The limitation in terms of number of ions is due to
145 space-charge effects, leading to frequency shifts, peak broadening and screening effects, which makes the re-centering
146 inefficient [23, 35]. As it is shown for example from simulations in [10], reducing the cloud density, i.e. expanding
147 the cloud for a given number of ions, is a way to limit these space-charge effects. By increasing the trap size, the field
148 anharmonicities are further from the center thus the cloud size can be larger. This is why the purification trap of PIPER-
149 ADE has a large diameter (64 mm) and aims at separating larger ion bunches (more than 10^4 ions). More recently,
150 promising variants of this sideband buffer gas cooling technique have emerged, such as the octupolar excitation for the
151 re-centering [36] or the so-called buffer-gas-free SIMCO excitation [37]. They will be studied using PIPERADE.

152 The purification trap will mostly be used for sideband buffer gas cooling, whereas the measurement trap could be
153 used for accumulation purposes. One can repeat the purification cycle by sending each time a newly cleaned sample to
154 the measurement trap, where He gas is injected for an efficient trapping. Once the accumulated sample is large enough
155 for a measurement, a final cleaning is needed to get rid of the daughter nuclei produced during the accumulation time
156 and the highly-purified sample of ions of interest can be sent to the downstream experiments.

157 The measurement trap could also be used for further high-resolution mass separation. With very few ions and in a
158 gas-free trap, other techniques can be used to reach a very high resolving power and separate close isobars or isomers.
159 The so-called dipole cleaning can be used by applying a dipolar field at the modified cyclotron frequency ν_+ of a well-
160 known contaminant, whose radius is increased enough to not be extracted from the trap. By applying time-separated
161 pulses, as described in the previous section, the so-called Ramsey cleaning is very powerful for a highly-selective
162 cleaning of a given contaminant. More details can be found in [19]. Such cleaning methods can reach resolutions up
163 to about 10^6 , which makes this technique also suitable for isomeric cleaning.

164 Finally, a very recent method, which has been implemented at JYFLTRAP for post-trap spectroscopy, is the phase-
165 splitting method, inspired by the Phase-Imaging Ion-Cyclotron-Resonance (PI-ICR) measurement technique [20]. De-
166 tails can be found in [21, 22]. The first step of this method is to excite the modified cyclotron motion of the trapped
167 ions by applying a short broad-band dipolar excitation. The excitation being short, it is not highly selective and the
168 radial amplitudes of all the isobars and any isomers are thus increased. Then the basic principle of this separation is
169 to let the ions oscillate at the fast modified cyclotron frequency ν_+ for a given time, so that the species are separated in
170 phase. This technique requires the use of a position-sensitive micro-channel plate (MCP) detector, in order to project
171 the radial position of the ion cloud on the detector. One should note here that extracting the ions moving at the higher
172 ν_+ frequency will lead to a smearing of the ion spot on the MCP. Therefore, before the ion extraction, a π -pulse excita-
173 tion has to be applied to convert the pure modified cyclotron motion into a pure magnetron motion, which then is slow

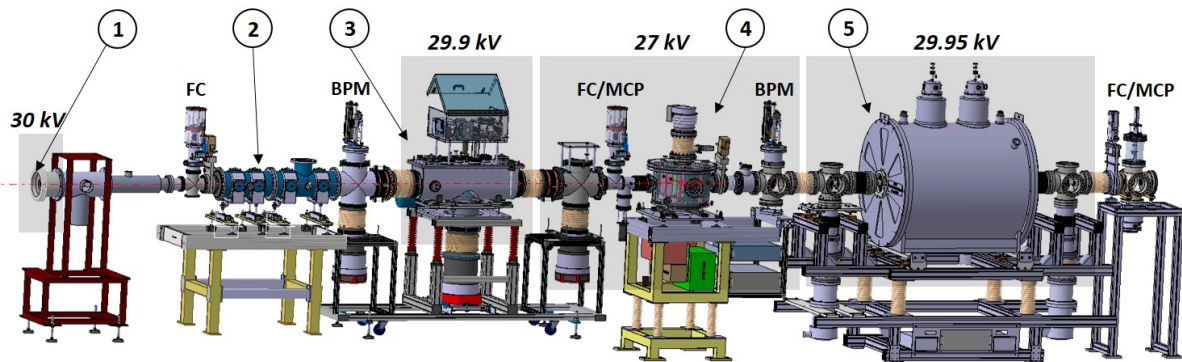


Figure 2: Experimental setup at CENBG, consisting of 1) a stable ion source floated at 30 kV, 2) a DESIR - quadrupole triplet, 3) the GPIB (General Purpose Ion Buncher) floated at about 29.9 kV, 4) an electrostatic deflector floated at 27 kV and 5) the 7-Tesla Penning-trap system floated at about 29.95 kV. Faraday cups (FC), beam profile monitors (BPM) and micro-channel plates (MCP) detectors are installed in the beam line for ion beam diagnostics.

174 enough to observe a well-defined spot on the detector. After the separation, the isobar or the state of interest can be
 175 transported to the post-trap spectroscopy device through a diaphragm with a hole at the appropriate angle and radius
 176 from the center. The selection method used at JYFLTRAP is to adapt the accumulation time so that the two species
 177 are separated by 180 degrees. A magnetron excitation in opposite phase with the motion of the ions of interest will
 178 center them in the trap while moving contaminants off-axis [22]. The selection method proposed in [21] is to apply a
 179 static excitation, to shift the center of the trap and then re-center the ions of interest. This has never been tested. The
 180 phase splitting method is very powerful in terms of resolution, which can even reach 10^7 for long accumulation times.

181 In the case of isomeric cleaning, before sending the isomeric beam to post-trap spectroscopy, the excitation energy
 182 of the isomeric state could also be measured with the techniques presented in the next section.

183 2.2.2. PIPERADE as a mass spectrometer

184 When using PIPERADE as a mass spectrometer, a highly-purified sample is required. Therefore both traps will still
 185 be used for various mass separations explained in the previous section before the precision mass measurement in the
 186 second trap is realized. The mass measurement of an ion is performed through the determination of its true cyclotron
 187 frequency $\nu_c = qB/2\pi m$. Once the cyclotron frequency is measured, only the magnetic field has to be measured to
 188 extract the mass of the ion. This is performed by alternatively measuring the cyclotron frequency of the ion of interest
 189 and that of a very well-known reference isotope. Even if the magnetic field is not monitored during the measurement
 190 of the ion of interest, if the field drift and fluctuations are small enough, a linear interpolation is sufficient, not to add
 191 systematic uncertainties to the measured mass.

192 The standard technique for cyclotron frequency determination used since decades is the ToF-ICR technique and is
 193 described in detail in [38]. The precision achieved with this method is of the order of 10^{-8} for short-lived nuclides.
 194 As for the dipole cleaning method, the Ramsey method has boosted this technique, with an increase of a factor of 3 in
 195 the precision on the mass determination [18].

196 A few years ago, the PI-ICR method has been introduced in the field and implemented in many Penning-trap mass
 197 spectrometers, such as SHIPTRAP [39] where it was first developed, CPT [40], ISOLTRAP [41] and JYFLTRAP [22].
 198 It has been shown to reach a fivefold gain for the precision on the cyclotron frequency determination compared to the
 199 Ramsey ToF-ICR technique. This non-scanning method opens the way to mass measurements of very exotic nuclei
 200 but also long-lived isomers, due to the excellent resolution it can reach (see the previous subsection).

201 3. Overview of the experimental setup at CENBG

202 The PIPERADE setup is currently being developed and commissioned at CENBG before its currently scheduled
 203 installation at DESIR/GANIL in 2024. A FEBIAD ion source is used to produce stable ions, either by ionizing a gas
 204 injected in the source, or by surface-ionizing the alkali naturally present on the filament surface. The injection into the
 205 Penning trap requires a bunched and cooled beam, mostly to optimize the transmission efficiency but also to reduce

206 the phase-space volume when trapping the ions. For this purpose, a gas-filled Radio Frequency Quadrupole (called
207 GPIB for General Purpose Ion Buncher) is also developed at CENBG. The GPIB will be installed on the entrance
208 beam line of the DESIR hall, acting as the main cooler-buncher of DESIR. Details on this device will be found in
209 [42]. As displayed in Figure 2, the PIPERADE setup is placed directly downstream of the GPIB. At its final position
210 at DESIR/GANIL, PIPERADE will be displaced in parallel to the GPIB and the main beam line. Ion bunches will
211 thus be sent to PIPERADE via a transfer line equipped with two 90° electrostatic deflectors. One of these electrostatic
212 deflectors has been constructed and installed at CENBG (see Figure 2) between the GPIB and PIPERADE devices for
213 test purposes (e.g. transverse and longitudinal emittance measurements).

214 As can be seen in Figure 2, the different devices are held on separate platforms electrically floated with respect to
215 the ion source potential of 30 kV. The difference of the GPIB and PIPERADE platforms to the main source platform
216 is tunable via 0 - 400V power supplies (DELTA Electronika SM1500) with negative polarity, one dedicated to each
217 platform. This allows to adjust the ion energy for an optimized injection in the devices (about 29.9 kV for the GPIB
218 and about 29.95 kV for PIPERADE). The transfer line from the GPIB to the PIPERADE setup through the deflector
219 is floated at 27 kV, to be in the same electrostatic configuration as in DESIR where the 3-keV ions will be deflected.
220 The ions extracted from the Penning-trap system are then accelerated to almost 30 keV and sent to a detection system
221 dedicated to tests or mass measurements. In the future, the ion bunches will be sent back to the main DESIR beam
222 line via a 45° bending.

223 Different beam optics systems are used to control the shape and the position of the beam all along the beam line: a
224 DESIR quadrupole triplet is located between the source and the GPIB to optimize the injection into the GPIB and an
225 einzel lens is located downstream the GPIB for an optimum injection of the beam into the magnetic field of PIPERADE.
226 In addition, sets of horizontal and vertical steerers are located upstream of both GPIB and Penning-trap devices, in
227 order to correct the angle and position of the ion beam. As can be seen in Figure 2, retractable beam profile monitors
228 are used to monitor the radial distribution and position of the ion beam injected in the GPIB and PIPERADE setups.
229 Three Faraday cups along the beam line are used to optimize the ion beam transmission efficiency in continuous mode.
230 When bunched with the GPIB, the ions are detected by micro-channel plates (MCP) detectors behind the GPIB at 27
231 kV and behind the traps at ground potential. The different beam diagnostics and their electronics are described in detail
232 in Section 4.3. The whole PIPERADE beam line, starting after the deflector, composed of DN160 crosses, bellows and
233 a DN125 vacuum tube inserted into the magnet, use the CF standard and a very low magnetic susceptibility stainless
234 steel (316L-1.4435). Two magnetically-levitated turbomolecular pumps (Edwards STP-1003) are located at both ends
235 of the setup, far from the magnet axis, as are the vacuum gauges. A third pump (Edwards STP-A803C) is located below
236 the MCP chamber after the trap system. The pressures at the injection and extraction sides, are 8×10^{-8} mbar and 1
237 $\times 10^{-8}$ mbar, respectively. The injection side pressure is higher because of the GPIB helium gas. It will be lower at
238 DESIR because the GPIB will be further upstream and additional pumping systems will be installed on the deflector
239 chambers. As it will be mentioned later, this pressure is higher when injecting He gas in the first trap. The pressure at
240 the MCP chamber is of the order of 10^{-8} mbar.

241 4. Technical description of the Penning-trap system

242 4.1. Double Penning trap

243 The double Penning trap of PIPERADE is shown in Fig. 1. As mentioned before, with a radius of 32 mm, the
244 purification trap is one of the largest Penning trap installed at any RIB facility (see [43] for details on the 90mm-radius
245 Penning trap of the TAMUTRAP facility), whereas the measurement trap has a radius of 10 mm. For both traps,
246 deviations from the ideal quadrupole field are compensated by correction electrodes added between the rings and the
247 endcaps electrodes. In addition, the dimensions of all electrodes and the voltages applied on them have been calculated
248 to limit the anharmonicities of the electric trapping potentials (see Tables 1 and 2).

249 As can be seen in Figure 1.a), the endcaps of the purification trap are 4 times axially segmented, to offer the
250 possibility to apply DC gradients at the injection and the extraction of the ions. In trapping configuration, they are all
251 at the same potential. In the radial direction, as can be seen in Figure 1.b), the purification trap and the measurement
252 trap have an 8-fold and 4-fold segmented central ring electrode, respectively, allowing to apply RF excitations. The
253 correction electrodes are also radially segmented (two parts) for implementing a broad-band Fourier-Transform Ion-
254 Cyclotron-Resonance (FT-ICR) detection [44], allowing a quick broad identification of the highly-abundant trapped
255 contaminants. Filters and pre-amplifiers boards are directly mounted on the trap structure inside the vacuum, in order
256 to reduce the noise of the very small induced current signal picked up on the electrodes. The full electronics system has

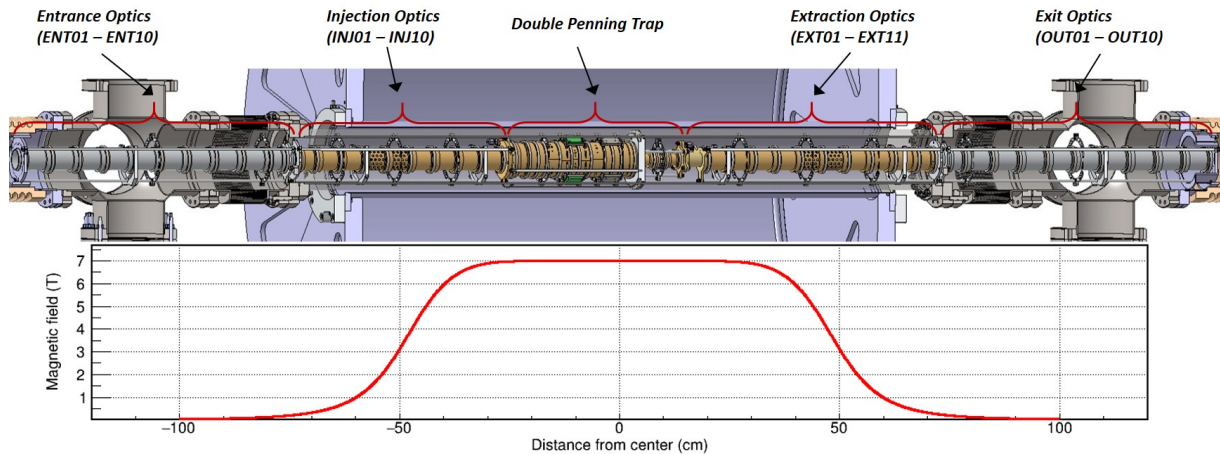


Figure 3: Top: Trap tower in the superconducting magnet consisting of injection/extraction optics and the double Penning trap separated by a diaphragm and entrance/exit beam optics on both sides of the magnet. Bottom: Magnetic field in Tesla along the trap tower.

257 been designed and built by Stahl-Electronics [45]. This detection technique has not been commissioned yet. Different
 258 diameters for the diaphragm have been machined in order to test different excitation patterns. The presently installed
 259 one has a 4 mm diameter. In addition, adaptation electrodes (see Figure 1.a) are added on both sides of the double
 260 Penning trap, in order to fix the optics electrodes towers, which have a different diameter than the traps. As mentioned
 261 earlier, the double Penning trap will be used in different configurations, which require He buffer gas, in one and/or the
 262 other trap. For that reason, the gas feedings to both traps are independent and consist of PEEK tubes connected to the
 263 adaptation electrodes via gas inlets, made of brass. Outside the vacuum, stainless steel gas tubes allow to transfer the
 264 gas from the two mass flow controllers (BROOKS SLA5850S) to the gas feedthroughs. With the present diaphragm
 265 diameter of 4 mm, when injecting He gas in the first trap, the pressure upstream the magnet measured by the gauge
 266 can be increased up to about 5×10^{-6} mbar without degrading the vacuum downstream the Penning-trap setup. Monte
 267 Carlo simulations using the Molflow+ software [46] have been performed to estimate the pressure inside the first trap
 268 cavity when He gas is injected, under the assumption of being in a molecular regime. A factor of 12 between the
 269 pressure measured by the gauge and the pressure inside the trap has been determined.

270 4.2. Tower structure

271 The trap tower structure located in the superconducting magnet is divided into 3 independent parts: the double
 272 Penning-trap structure and two sets of 10 and 11 cylindrical electrodes for the injection and the extraction of the ions,
 273 respectively, in the critical areas of the magnetic field gradients (see Figure 3). On both sides of the double Penning
 274 trap, the last injection electrode and the first extraction electrode are specific adaptation electrodes (see Figure 1.a),
 275 with the same radius as the traps, to fix the optics electrodes, which all have a radius of 20 mm and 51 mm length.
 276 The full tower has been designed and machined at the Max Planck Institut für Kernphysik (MPIK) in Heidelberg, Germany.

277 The measurement trap electrodes and the diaphragm are made of oxygen-free copper, chosen for its high con-
 278 ductivity and low magnetic susceptibility. All the injection, extraction and purification trap electrodes are made of
 279 aluminum alloy (AW-5083), a compromise to have a reasonable weight, critical for a precise alignment and for an
 280 easier assembly of the full structure. The aluminum electrodes have first been plated with a 5- μ m copper layer, and all
 281 the electrodes have then been silver (15 μ m) and gold (5 μ m) plated. The gold layer is to prevent oxidation whereas the
 282 silver one prevents gold from diffusing into the copper material. In general, a tolerance of ± 30 μ m has been achieved
 283 for the dimensions of all the electrodes. All electrodes are insulated from each other by MACOR[®] rings. The tower
 284 electrodes are designed in such a way that the insulator rings cannot be seen by the ions (see Fig.1.a). Concerning the
 285 radially-segmented electrodes, the segments are insulated from each other by sapphire balls of 1.5 mm diameter. The
 286 kapton-insulated wires are connected to each electrode with M2.5 titanium screws. This tower is inserted in a DN125
 287 vacuum tube and held via three rods screwed on metal landmarks soldered on the flanges at each extremity of the tube.
 288 Since the tower is thus radially and axially self-aligned in the tube, the latter can then be aligned in the magnet thanks

Electrode	Length (mm)
Purification trap ($r = 32$ mm)	
Endcap 1 (PE1)	30.0
Endcap 2 (PE2)	17.5
Endcap 3 (PE3)	17.5
Endcap 4 (PE4)	30.0
Correction 1 (PC1)	25.1
Ring (PR)	9.310
Correction 2 (PC2)	25.1
Endcap 5 (PE5)	30.0
Endcap 6 (PE6)	17.5
Endcap 7 (PE7)	17.5
Endcap 8 (PE8)	30.0
Diaphragm ($r = 2$ mm)	30
Measurement trap ($r = 10$ mm)	
Endcap 1 (ME1)	29.7
Correction 1 (MC1)	7.185
Ring (MR)	2.224
Correction 2 (MC2)	7.185
Endcap 2 (ME2)	29.7

Table 1

Dimensions (in mm) of the trap electrodes. The electrodes are separated from each other by a gap of 1 mm.

289 to screws from a special system fixed to the magnet in vertical and horizontal directions. The radial alignment will
 290 be described in section 4.6.3. In addition to the main trap tower, two other 10-electrode towers are installed on each
 291 side of the superconducting magnet, in the regions of deceleration/acceleration of the ions, and were also designed and
 292 manufactured at MPIK. They are made of aluminum alloy and have a radius of 20 mm and 60 mm length.

293 4.3. Beam diagnostics and detectors

294 Monitoring the ion beam is crucial to optimize the beam line and the in-trap techniques. As the trap device is
 295 on a high-voltage platform, there is no pulsed drift tube, the transmission efficiency can thus be optimized with a
 296 continuous beam along the whole beam line. To do so, three movable Faraday cups (FC) are installed in the beam line,
 297 as can be seen in Figure 2. These are DESIR-standard FC developed by GANIL, covering a very wide range of current
 298 intensities, from only 50 fA to 100 μ A. To achieve such a high sensitivity, each FC is coupled to a low-bandwidth
 299 transimpedance linear amplifier called PicoLIN [47], also developed by GANIL within the SPIRAL2 project. The
 300 beam position, size and shape is monitored with SPIRAL2 beam profile monitors (BPM), based on secondary electron
 301 emission of 47 tungsten wire harps (0.5 mm step) for both horizontal and vertical planes [48]. Equipped with high-
 302 sensitivity charge preamplifiers, these semi-interceptive BPM are used to monitor down to a few tens of pA ion beams
 303 with a transparency higher than 90%.

304 Ion bunches generated by the GPIB can be detected by the FC, coupled to a fast commercial I/V converter (FEMTO
 305 DHPA-100). This detection system can be used only for high-intensity bunches ($> 10^4$ particles in a 1 μ s bunch),
 306 the lower ion number limit strongly depending on the time distribution of the bunch. The voltage image of the bunch
 307 intensity is digitized with a Red Pitaya board, which is also controlling the amplifier using digital I/O (switchable gain
 308 from 10^2 to 10^8 V/A). The Red Pitaya board is a cost-efficient data acquisition platform based on a Xilinx FPGA and
 309 a dual-core ARM processor running a Linux operating system. Amplifier output signal sampling and quantization are
 310 achieved with a 14-bit ADC at 125 MSample/s in parallel with the digital I/O processing without any dead time. The
 311 Australian Synchrotron EPICS driver support is used to run the Faraday Cup EPICS server (see section 4.5) in the Red
 312 Pitaya itself [49].

313 In case of low-intensity bunches, there are two MCP's (Topag MCP-MA33/2) installed in the beam line, one after
 314 the GPIB and one after the Penning-trap setup. They allow measuring the absolute number of ions in a bunch as well
 315 as performing time-of-flight measurements. The MCP anode signal is discriminated and a specific counting system
 316 has been developed. This FPGA development called RedPiTOF has been implemented into a dedicated Red Pitaya.
 317 Thanks to the use of two digital inputs (MCP counts and bunch gate signals), it allows to benefit from 50 MHz counters,

318 time measurements with 10 ns time resolution and TOF spectrum construction in 16k channels without any dead time.
319 The modified embedded EPICS server (see section 4.5) allows from any EPICS Client to monitor online the MCP
320 counting rate, the number of counts per bunch and the TOF spectrum. More details about this new development will
321 be presented in a dedicated paper, under preparation.

322 A position-sensitive MCP (delay-line detector) is planned to replace the MCP after the trap, in order to implement
323 the phase-splitting [21, 22] and PI-ICR [20] methods described in section 2.2.

324 4.4. Trap electronics

325 In order to meet the DESIR High Voltage-Power Supplies (HV-PS) requirements, ISEG multichannel crates are
326 used for providing the DC voltages to the DESIR instruments. The reasons of such a choice are (i) the large variety of
327 low-noise, precise and stable HV-PS proposed, (ii) its ability to concentrate a large number of HV channels in a single
328 crate, and (iii) the CC-24 ISEG crate controller with its built-in EPICS server (see section 4.5). A SPIRAL2-like EPICS
329 records database is developed and used on all DESIR ISEG crates. The PIPERADE electronics stands in a dedicated
330 19" rack placed on a 29.95 kV platform and require 75 HV-PS, all with negative polarity. The DC signals for the trap
331 electrodes and the diaphragm are provided by 0 - 500V high-precision supplies (ISEG EHS-F205N). The injection and
332 extraction electrodes are supplied by 0 - 1kV modules (ISEG EHS F010n) whereas the entrance and exit electrodes on
333 both sides of the magnet are supplied by 0 - 6kV modules (ISEG EHS F060n). The switching of the trapping potentials
334 is required to be fast, in order to capture efficiently the ions and to extract them from the traps without degrading their
335 energy distribution. This is performed by homemade fast switches (see [42] for more details), capable of switching up
336 to 100 V in about 30 ns. The RF fields for the different motion excitations are supplied by Agilent 33510B function
337 generators with a 1 μ Hz frequency resolution. The ring electrode of both traps being supplied by both RF and DC
338 signals, AC/DC couplings are performed before the connection to the trap electrodes. Another main instrument used
339 as the conductor of the traps has been developed on a National Instruments CompactRIO device: the Pulse Pattern
340 Generator (PPG). This real-time and FPGA-based device triggers the function generators and the fast switches with
341 respect to a given time pattern defined by the users with a 12 ns time resolution. Ion bunch injection, trapping, cooling
342 and excitation times, ion bunch transfer and extraction are controlled by this PPG.

343 4.5. Control system

344 Control System (CS) developments performed at CENBG for DESIR are based on the Experimental Physics and
345 Industrial Control System (EPICS) architecture [50], being the basic framework for the SPIRAL2 control system [51].
346 PIPERADE is therefore also fully remotely controlled under EPICS. This system is based on Clients (Operator Inter-
347 faces) and Servers (Input Output Controllers IOC) communicating together via shared Process Variables (PVs) on an
348 Ethernet Network using a dedicated communication protocol named Channel Access (CA). Most of the PIPERADE
349 electronics is embedded on a high-voltage platform. Therefore, fiber optics coupled to Ethernet switches ensure gal-
350 vanic insulation and TCP communication of the equipment with the EPICS IOCs running on a CentOS Linux PC. Some
351 IOCs are embedded into the equipment: this is the case for the ISEG HV multichannel crate (ISEG CC24 Controller)
352 and the Red Pitaya used for beam intensity, ion counting and time-of-flight (RedPiTOF) measurements. SPIRAL2
353 vacuum systems and interlocks are controlled using dedicated PLCs (Siemens S7-1500). The Profibus Fieldbus is
354 used by the vacuum PLC to communicate with turbo-molecular pumps and Profinet (Profibus on Ethernet Network) is
355 deployed to manage Input-Output terminal modules (ET 200S) distributed along the beam line and on the high-voltage
356 platforms. Each PLC has its own HMI (Human Machine Interface) on a dedicated Touch Panel.

357 Shared software development tools are used such as the SPIRAL2 version of CSS/BOY (CSS-Dev) used to build
358 most of the Graphical User Interfaces (GUIs) and will handle central services like the data archiver or the alarm handler
359 system in the near future. EPICS with its CA protocol makes possible to monitor and control any beam line equipment
360 through its PVs in many programming languages. Using this EPICS feature, a Python program is under development
361 to operate the traps, i.e. scan the different trapping and excitation parameters, control the PPG and read on-line output
362 data from the RedPiTOF instrument. Bunch counts and TOF spectra are processed and plotted as a function of the
363 scanned parameters. It is inspired by the PyMassScanner program [52] developed at JYFLTRAP.

364 4.6. Superconducting magnet

365 The superconducting magnet is a 7-Tesla magnet manufactured by CRYOGENIC [53], consisting of a set of NbTi
366 windings immersed in liquid helium at 4.2 K. The main magnet has a 160 mm room-temperature bore in which the
367 vacuum tube is installed and a cryostat with an overall diameter of 1112 mm and a length of 1250 mm. It has a 500

368 liter helium reservoir suspended within the cryostat vacuum space by stainless steel necks attached inside the turrets,
369 surrounded by a 125 liter annular nitrogen reservoir. The main coil has been loaded to 118 A, leading to a magnetic
370 field of 7 Tesla. There is also an independent active shield coil wound onto the main winding magnet where no current
371 is applied. However, a low current created by inductive coupling to the main coil is increasing with time, and might
372 slightly modify the magnetic field. Therefore, every few months or before a precision measurement, the current on this
373 coil has to be released. Two other superconducting compensation coils connected to the main coil, i.e. with the same
374 current, are positioned on both ends of the magnet, allowing a first rough compensation of the inhomogeneity along
375 the magnet axis. In addition, there are two sets of superconducting shim coils, allowing to adjust independently the
376 homogeneity over two specific regions separated by 20 cm, corresponding to the two trap regions. Each set of coils
377 has three 1st-order shim coils in the three directions X, Y and Z and an additional 2nd-order shim coil in Z direction
378 (magnet axis) to compensate non-linear inhomogeneities.

379 **4.6.1. Field homogeneity**

380 The field homogeneity in the trapping region is crucial because the radial motion frequencies as well as the true
381 cyclotron frequency depend on the magnetic field. As ion motions have non-zero amplitude, any inhomogeneity of
382 the field in the space where the motions take place leads to frequency shifts, resulting in a loss of resolving power in
383 mass separation or precision in mass measurements. The shimming has been done by adjusting currents of the order
384 of a few ampere on X and Y shim coils for radial shimming, and on the Z shim coil for axial shimming. The 2nd-order
385 coils were finally not needed for the adjustment. Since the latter have a strong inductive coupling to the main magnet,
386 having in principle no current on these shim coils allows us to release from time to time, as for the shield coil, the
387 accumulated induced current. An NMR probe coupled to a precision teslameter (Metrolab PT2025) has been used
388 to precisely measure the magnetic field along the axis and around the two trap center regions. Figure 4 shows the
389 magnetic field homogeneity, i.e. the relative deviation from the centers of the trapping regions, separated by 20 cm. A
390 wider region is shown for PT (purification trap), which has larger dimensions, and where ions will move further from
391 the trap center. Even over a very large region of 10 mm radius and 20 mm length the homogeneity is still of the order
392 of 3 ppm. On the MT (measurement trap) side, an homogeneity below 1.3 ppm has been obtained over a region of 5
393 mm radius and 10 mm length.

394 One should note that with the NMR-probe installed in the vacuum tube, the homogeneity determination was per-
395 formed without the trap electrodes inserted in the tube. However, as it is described in Section 4.1, all materials were
396 carefully chosen to be of very low magnetic susceptibility, so as not to induce any additional field inhomogeneity.

397 **4.6.2. Field drift**

398 Due to the so-called flux creep phenomenon [54], the magnetic field decreases over time. The active shield coil
399 allows to reduce this drift from 0.13 ppm/h to 0.04 ppm/h. However, for precision mass measurements, this drift is still
400 too high. Therefore, an additional warm coil has been added afterwards in the magnet bore, allowing to compensate
401 very precisely the linear drift by applying a ramp of the order of +100 μ A/h. This has been tested with the NMR-probe
402 located at the center of the measurement trap's region and showed that the field drift can be reduced by about two
403 orders of magnitude, as can be seen in Figure 5. Due to the limited precision of the NMR-probe and the sensitivity of
404 the teslameter to temperature fluctuations, this will have to be determined more precisely with the cyclotron frequency
405 of trapped ions.

406 **4.6.3. Tube alignment with respect to the magnetic field**

407 Another cause of ion frequency shifts is a misalignment between the electric trapping field and the magnetic field
408 axes. The way the main coil is suspended in the cryostat does not guarantee a perfect alignment of the coil in the main
409 magnet structure. The coil also slightly moves when cooling the magnet, therefore the alignment procedure has to be
410 performed when the magnet is warmed up and cooled again, i.e. after the move of the setup to GANIL.

411 The trap electrodes are mechanically aligned in the vacuum tube but this assembly must be aligned with the mag-
412 netic field axis. The option to move the vacuum tube with respect to the magnetic field axis has been chosen. It prevents
413 moving the magnet while it is cold, which can be risky.

414 A standard procedure using an electron-gun device inserted in the vacuum tube has been used (see Figure 6). By
415 heating a tungsten ribbon positioned at the center of the magnet with a current of 10-15 A and by floating it to a
416 potential of about -50 V, low-energy electrons are created and thus spiral closely around the magnetic field lines on
417 both sides of the magnet. Two plates with apertures of 0.5 mm diameter each fixed on both sides of the filament and

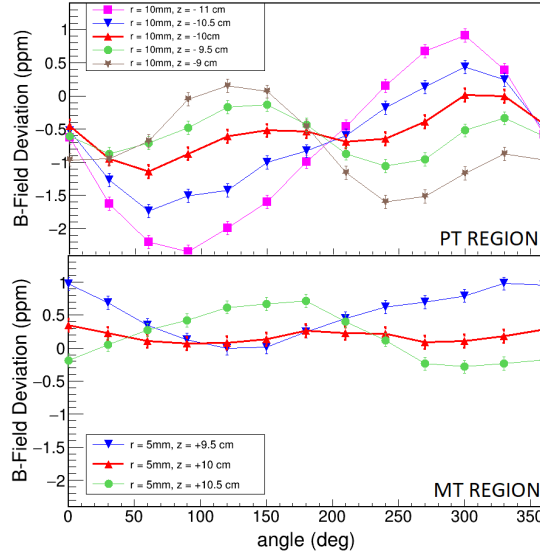


Figure 4: Relative azimuthal magnetic field deviation from the centers of the PT (purification trap) and MT (measurement trap) trapping regions. The centers of these regions are at $r = 0$, $z = -10$ cm and $z = +10$ cm, for the PT and MT regions, respectively. Deviations are shown for different azimuth angles at a radius of 10 mm and over 20 mm length for the PT region and at a radius of 5 mm and over 10 mm length for the MT region. For both regions, the red bold lines correspond to the axial centers of the trapping regions.

418 at a distance of 15 mm, define the initial shape and size of the electron beam. Detectors are placed at both ends of the
 419 magnet, each of them consisting of a metallic plate acting as a Faraday cup on which another 8-fold segmented plate
 420 (4 inner quadrants surrounded by 4 outer ones) with a 0.5 mm pinhole in the center is fixed. The aim of the procedure
 421 is to move the vacuum tube in such a way that the electron beam travels through the pinhole in the first layer of the
 422 detector and thus the electron current on the main detection plate is maximized. The segments of the first plate allow
 423 to estimate the position of the beam. The further the detectors are from the filament, the more precise is the alignment.
 424 However, starting the procedure with very far detectors is not convenient if the beam is not observed at all. Therefore,
 425 the two sets of detectors were mounted on elements sliding on rods, such that the axial position of the detectors could
 426 be controlled by a crank from outside the vacuum (see Figure 6), so that the setup does not have to be opened every
 427 time the position has to be changed.

The vacuum tube inclination was finally corrected by 2.7(13) mrad. It is thus not perfectly aligned with the rest of the beamline anymore, but now well aligned with the magnetic field axis. The resulting cyclotron frequency shift from the possible remaining angle can be calculated from the formula given in [55, 56]:

$$\Delta\nu_c = \frac{9}{8\pi}\nu_-\theta^2 \quad (2)$$

with θ the angle between the electric and magnetic field axes and ν_- the magnetron frequency of the trapped ions, being expressed, in first-order approximation, as $\nu_- = U_0/(4\pi d^2 B)$. One can notice from the Equation 2 that the absolute frequency shift is, in first-order, mass-independent. As explained in the following section, the trap parameter d^2 can be determined from the simulated electric field and is equal, for the measurement trap, to 134.49 mm². With $\theta = 1.3$ mrad, corresponding to the uncertainty on the angle, the resulting cyclotron frequency shift in the second trap will be from 0.5 mHz for a trapping potential of 10 V, to 5 mHz for a trapping potential of 100 V. The relative uncertainty on the true cyclotron frequency ν_c depends then on ν_c itself, the heavier the mass the larger the uncertainty. However, as it is explained in Section 2.2, the cyclotron frequency of an ion of interest ν_c is always measured relatively to a well-known reference ion with a cyclotron frequency ν_c^{ref} . Therefore, the resulting relative uncertainty we are interested in is the

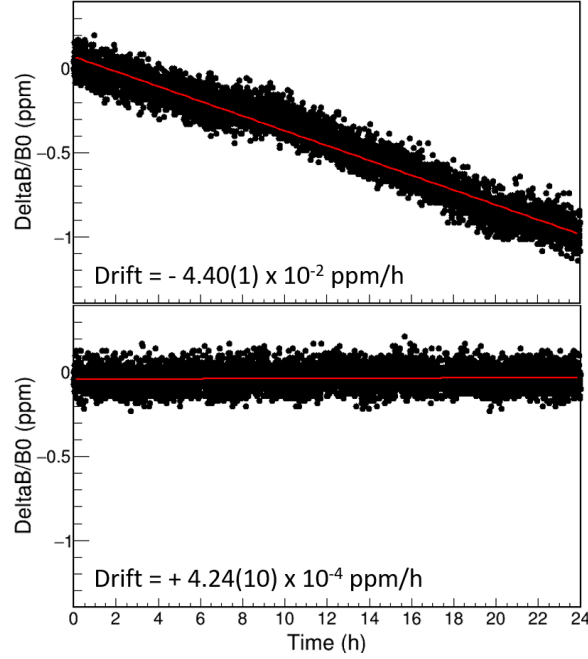


Figure 5: Magnetic field B relative to the initial magnetic field B_0 as a function of time. The red lines correspond to a fit of the data to a linear function ; the resulting slope is shown on the Figure. Top: No current is applied on the additional warm coil. Bottom: A positive ramp current is applied on the warm coil.

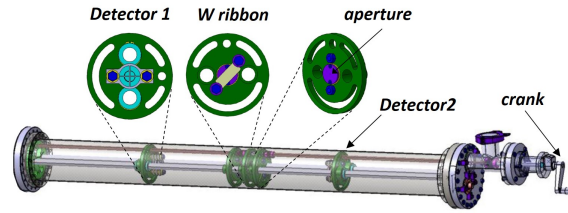


Figure 6: Electron gun device installed in the vacuum tube, consisting of a tungsten ribbon in the center, apertures on both sides, as well as 8-fold segmented detectors with a hole and a plate behind. A crank connected to a worm gear is used to change the axial position of the detectors with respect to the filament.

one on the ratio $r = v_c/v_c^{ref}$. In [56], it is given by the formula:

$$\frac{\delta r}{r} = \frac{9}{4}\theta^2 \frac{v_-}{v_+^{ref}} \left(\frac{v_+^{ref} - v_+}{v_+} \right) \quad (3)$$

By assuming that $v_+ \approx v_c$ for both the ions of interest and the reference ions, one can simplify the Equation 3 and define a shift factor R depending only on the trap parameters, the magnetic field strength and the misalignment of the magnetic field to the trap axis. For a mass measurement, the relative uncertainty will then be given by the trapping potential U_0 and the mass difference between the ions of interest and the reference ions ΔA :

$$\frac{\delta r}{r} = R \cdot U_0 \Delta A = \frac{9}{4}\theta^2 \frac{1}{2d^2 B^2} \frac{u}{q_e} \cdot U_0 \Delta A \quad (4)$$

with u the atomic mass unit and q_e the elementary charge (assuming all trapped ions are of 1^+ charge state). The final

Electrode	Voltage(V)
ENT01 - ENT10	from -2950 to -1000
INJ01 - INJ10	from -800 to -85
Purification trap	Open/Closed
Endcap 1 - Endcap 4 (PE1 - PE4)	-84 / 0
Correction 1 (PC1)	-82 / -70
Ring (PR)	-80 / -80
Correction 2 (PC2)	-82 / -70
Endcap 5 - Endcap 8 (PE5-PE8)	-84 / 0
Diaphragm/Measurement trap	from -85 to -90
EXT01 - EXT11	from -100 to -120
OUT01 - OUT10	from -130 to -3000

Table 2

Voltages (V) applied to the entrance electrodes (ENT01-ENT10), the injection electrodes (INJ01-INJ10), the extraction electrodes (EXT01-EXT11) and the exit electrodes (OUT01-OUT10). For the purification trap, voltages (V) applied in "opening mode", i.e. when the ions are either injected in the trap (voltages from PE1 to PR) or extracted from the trap (voltages from PR to PE8), and in "closed" mode, i.e. when ions are trapped. The setup and the power supplies are installed on a high-voltage platform. All these voltages are thus relative to the platform reference.

relative uncertainty resulting from an angle of 1.3 mrad between the magnetic and electric field axes is:

$$\frac{\delta r}{r} = 3.0 \times 10^{-12} V^{-1} \cdot U_0 \Delta A \quad (5)$$

428 Even with a trapping potential U_0 of 100 V and a ΔA of 10, the relative uncertainty of 3.0×10^{-9} is still negligible on
429 the level of the expected precision of the Penning trap, i.e. of the order of 10^{-8} for short-lived ions.

430 5. First offline tests with the purification trap

431 We report here the first offline tests of the PIPERADE mass spectrometer. As no gas was injected in the stable ion
432 source, the ion beam consisted only of surface-ionized elements. The ion beam was first cooled and bunched by the
433 GPIB, with RF parameters set to transmit light ions, such as $^{39}\text{K}^+$ or $^{40}\text{Ca}^+$, and then sent to the PIPERADE traps. A
434 so-called beam gate was implemented using one of the steerers at the exit of the ion source. Switching this electrode
435 for a short moment allows to inject in the GPIB a well-defined number of ions, and also to avoid the GPIB to be fed
436 constantly with "hot" ions that mix with the cold ones when extracting an ion bunch.

437 The ion bunches are extracted from the GPIB floated at 29.9 kV towards the deflector at 27 kV with an energy of
438 about 2.9 keV, and are then sent to the Penning-trap platform, which is at 29.95 kV. In order to attenuate the strong
439 defocusing effect of the platform voltage change from 27 kV to 29.95 kV and a abrupt drop of the ion energy, the
440 first entrance electrodes are set at about -2950 V, and then a smooth gradient is applied, in order to decelerate the ions
441 for the injection in the purification trap, where the ion energy has to be lower than the trapping potential, in this case
442 80 V. Table 2 shows the voltages applied on the different electrodes. For the purification trap electrodes, "Open" and
443 "Closed" correspond to the settings for injection/extraction and trapping modes, respectively. For the first tests, the
444 four axial segments of each endcap were all connected together.

445 Before performing any trapping in the purification trap, the bunches were shot through the Penning trap tower and
446 detected on the MCP detector behind the setup. The absolute transmission efficiency through the trap device is difficult
447 to determine, because the MCP's before and after the traps have not been precisely calibrated and despite the fact they
448 are identical, they might have slightly different detection efficiencies. This is mostly due to different time and spatial
449 distributions of the bunches hitting the detector leading to different saturation effects, but also due to the difference in
450 ion energy (3 keV after the GPIB and 30 keV after PIPERADE) and the fact that there are grids in front of the GPIB
451 MCP (to measure the bunch energy dispersion) which might impact the detection efficiency. A test bench with another
452 offline ion source is being mounted in the hall of CENBG, in order to precisely calibrate the detectors, depending on
453 the ion beam conditions. Despite the difficulty of precisely determining the efficiency, the number of counts/bunch
454 detected on the MCP after the GPIB and on the one after PIPERADE were similar for a given beam gate duration,
455 which shows that the overall transmission efficiency is excellent, most probably above 30-50%. One should note that

456 in continuous mode, by detecting the beam on the Faraday cups, the transmission efficiency through the traps has been
 457 estimated to about 60-70%. All these efficiencies will more precisely be measured during the on-going commissioning.

458 The trapping mode has then been tested. In order to capture the ions coming from the GPIB, the injection endcaps
 459 (PE1-PE4) are open while the extraction endcaps (PE5-PE8) are kept closed. Then, when the ions reach the trap center,
 460 the injection endcaps have to be closed, i.e. switched up to 0 V. The capture efficiency can be determined by the ratio
 461 of the number of counts of the MCP detector after a trapping cycle to the number of the counts in "shooting-through"
 462 mode, i.e. without any trapping. This has been determined to be >80% and is reliable because the MCP detector is the
 463 same one for both measurements.

464 The first sideband buffer gas cooling technique was performed with the following time pattern:

- 465 1) Extraction from the GPIB (triggers the PPG of the trap)
- 466 2) Waiting time while the ions fly from the GPIB to the PT (62 μ s)
- 467 3) Closing of the injection endcaps and first correction electrode
- 468 4) Axial cooling time (200 ms)
- 469 5) Dipolar magnetron excitation (15 ms)
- 470 6) Quadrupolar cyclotron excitation (200 ms)
- 471 7) Waiting time for cooling (200 ms)
- 472 8) Opening of the extraction endcaps and second correction electrode
- 473 9) Trigger for the MCP detection gate

474
 475 As can be seen from the above time pattern, after the capture of the ions, a waiting time is needed to axially cool
 476 the ions before applying the magnetron excitation. This time is strongly dependent on the amount of buffer gas injected
 477 in the trap, the higher the pressure the shorter the time.

478 The magnetron excitation was first tested, meaning that step 6 was omitted. The dipolar field was applied during
 479 10 magnetron periods with an amplitude of 2.2 Vpp. Figure 7 shows the number of counts/bunch detected on the
 480 MCP detector behind the trap as a function of the frequency of the RF excitation. We can see that at the resonance
 481 frequency ν_- , the counts/bunch drops to zero because the ion's magnetron radius has been increased to an orbit higher
 482 than the diaphragm radius, and thus no ions can be extracted from the trap. The amplitude of the magnetron excitation
 483 was tuned, so that it is high enough to radially push the ions beyond the diaphragm, but low enough so that the ions
 484 are not too far from the center. The further they are, the harder it is to re-center them because of frequency shifts
 485 induced by anharmonicities of the electric field and inhomogeneities of the magnetic field. The magnetron frequency
 486 has been determined to be about 660 Hz. This is in perfect agreement with the magnetron frequency calculation from
 487 the formula $\nu_- = U_0/(4\pi d^2 B)$, with $d^2 = 1360.90 \text{ mm}^2$ determined from a linear fit of the trap electric field simulated
 488 by SIMION [57] (see Eq. 1). The geometric formula for the characteristic trap parameter $d = \sqrt{z_0^2 + r_0^2}/2$ is actually
 489 not correct anymore for a real cylindrical Penning trap. All these offline tests were performed with He gas injected
 490 in the trap, giving a pressure of 2.6×10^{-7} mbar on the injection side of the magnet. From the Molflow simulations

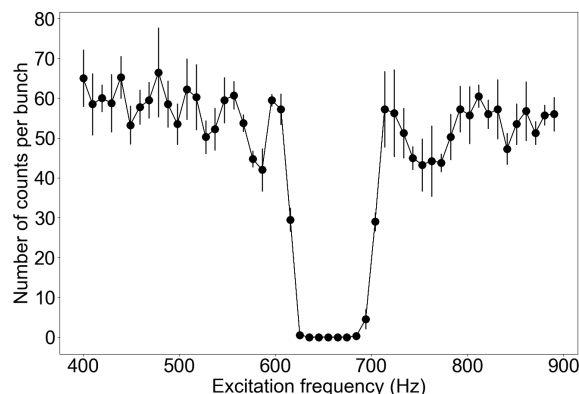


Figure 7: Number of counts/bunch detected on the MCP detector behind the trap as a function of the frequency of the dipolar magnetron excitation.

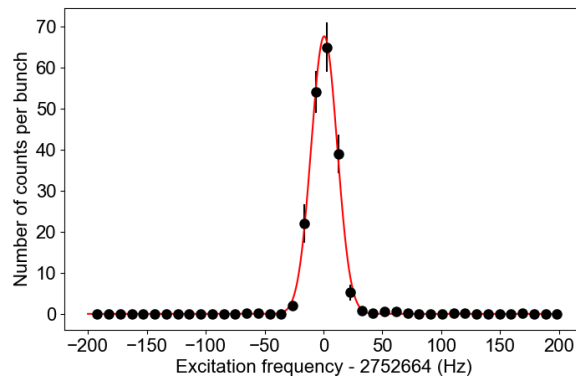


Figure 8: Number of counts/bunch detected on the MCP detector behind the trap as a function of the frequency of the quadrupolar RF excitation. At the resonance frequency ν_c , $^{39}\text{K}^+$ ions are centered in the trap. The gaussian fit to the data, shown in red, has a sigma of 11.0 Hz

described in Section 4.1, the pressure inside the trap cavity was then of the order of 3×10^{-6} mbar.

A quadrupolar excitation of 200 ms duration was then applied (step 6 in the above time pattern) with 2 Vpp amplitude, in order to re-center the ions. Figure 8 shows the number of counts/bunch detected on the MCP detector behind the trap as a function of the quadrupolar excitation RF frequency. This first resonance allows to confirm that $^{39}\text{K}^+$ ions are indeed produced from the ion source. The resonance curve was fitted with a Gaussian function, resulting in a sigma of 11.0 Hz. With a FWHM of about 26 Hz, the resolution ν_c/FWHM is then 106 000. The targeted resolution of this technique has thus been achieved. Studies are on-going to investigate the evolution of the resolution and the re-centering efficiency with respect to the different excitation parameters. The magnetron and cyclotron excitation amplitudes, as well as the amount of gas and the different pattern step times are strongly correlated and they all affect the sideband buffer-gas cooling performances. The next step is then to study separation performance as a function of the total number of trapped ions and for different ratios between the ions of interest and the contaminants.

6. Conclusions and outlook

A double Penning trap has been developed for mass separation and mass spectrometry at the future DESIR/SPIRAL2 facility. The installation of this device at CENBG has been finalized and is now under commissioning. First offline tests using the purification trap have shown that a resolution of 10^5 can be achieved. The next main step is to implement the mass spectrometry and high-resolution separation techniques for the measurement trap of PIPERADE. The first on-line experiments at DESIR with PIPERADE are foreseen in 2026.

Acknowledgements

The authors would like to thank the JYFLTRAP team for providing the PyMassScanner program, and in particular T. Eronen for all the fruitful discussions. Contributions from H. Guérin, M. Aouadi, P. Dupré and S. Stahl are gratefully acknowledged. The authors also thank the MPIK mechanical workshop and design office, as well as the CENBG mechanical workshop. The PIPERADE project was supported by Agence Nationale de la Recherche (ANR-2011-BS04-020-02 and ANR-11-EQPX-0012) and the Max Planck Society.

References

- [1] H. Kluge, Penning trap mass spectrometry of radionuclides, *Int. J. Mass Spectrom.* 349 (2013) 26, <https://doi.org/10.1016/j.ijms.2013.04.017>.
- [2] T. Eronen, et al., Ion traps in nuclear physics - Recent results and achievements, *Prog. in Part. and Nucl. Phys.* 91 (2016) 259, <http://dx.doi.org/10.1016/j.pnpnp.2016.08.001>.
- [3] M. Mukherjee, et al., ISOLTRAP: An on-line Penning trap for mass spectrometry on short-lived nuclides, *Eur. Phys. J. A* 35 (2008) 1, <https://doi.org/10.1140/epja/i2007-10528-9>.

- 521 [4] T. Eronen, et al., JYFLTRAP: a Penning trap for precision mass spectrometry and isobaric purification, *Eur. Phys. J. A* 48 (2012) 46. doi:
522 10.1140/epja/i2012-12046-1.
- 523 [5] R. Ringle, et al., Penning trap mass spectrometry of rare isotopes produced via projectile fragmentation at the LEBIT facility, *Int. J. Mass*
524 *Spectrom.* 349-350 (2013) 87–93, <https://doi.org/10.1016/j.ijms.2013.04.001>.
- 525 [6] A. Kwiatkowski, et al., Precision mass measurements at TITAN with radioactive ions, *Nucl. Instrum. Methods Phys. Res. B* 317 (2013) 517,
526 <https://doi.org/10.1016/j.nimb.2013.05.087>.
- 527 [7] M. Block, et al., Towards direct mass measurements of nobelium at SHIPTRAP, *Eur. Phys. J. D* 45 (2007) 39, <https://doi.org/10.1140/epjd/e2007-00189-2>.
- 529 [8] G. Savard, et al., Studies of neutron-rich isotopes with the CPT mass spectrometer and the CARIBU project, *Int. J. Mass Spectrom.* 251 (2006)
530 252, <https://doi.org/10.1016/j.ijms.2006.01.047>.
- 531 [9] J. Grund, et al., First online operation of TRIGA-TRAP, *Nucl. Instrum. Methods Phys. Res. A* 972 (2020) 164013, <https://doi.org/10.1016/j.nima.2020.164013>.
- 533 [10] P. Ascher, et al., PIPERADE: A Penning-trap isobar separator for the DESIR low-energy facility of SPIRAL2, *EPJ Web of Conf.* 66 (2014)
534 11002, <https://doi.org/10.1051/epjconf/20146611002>.
- 535 [11] E. M. Ramirez, et al., Conception of PIPERADE: A high-capacity Penning-trap mass separator for high isobaric contamination at DESIR,
536 *Nucl. Instrum. Methods Phys. Res. B* 376 (2016) 298, <https://doi.org/10.1016/j.nimb.2016.01.044>.
- 537 [12] B. Blank, S. Grévy, P. Thirolf, C. Weber, Perspectives for mass spectrometry at the DESIR facility of SPIRAL2, *Int. J. Mass Spectrom.* 349
538 (2013) 264, <https://doi.org/10.1016/j.ijms.2013.03.006>.
- 539 [13] <https://heberge.cenbg.in2p3.fr/desir>.
- 540 [14] P. Delahaye, et al., New exotic beams from the SPIRAL1 upgrade, *Nucl. Instrum. Methods Phys. Res. B* 463 (2020) 339, <https://doi.org/10.1016/j.nimb.2019.04.063>.
- 542 [15] F. Déchery, et al., The Super Separator Spectrometer S3 and the associated detection systems: SIRIUS and LEB-REGLIS3, *Nucl. Instrum.*
543 *Methods Phys. Res. B* 376 (2016) 125, <https://doi.org/10.1016/j.nimb.2016.02.036>.
- 544 [16] T. Kurtukian-Nieto, et al., SPIRAL2/DESIR high resolution mass separator, *Nucl. Instrum. Methods Phys. Res. B* 317 (2013) 284–289,
545 <https://doi.org/10.1016/j.nimb.2013.07.066>.
- 546 [17] G. Savard, et al., A new cooling technique for heavy ions in a Penning trap, *Phys. Lett. A* 158 (1991) 247, [https://doi.org/10.1016/0375-9601\(91\)91008-2](https://doi.org/10.1016/0375-9601(91)91008-2).
- 548 [18] S. George, et al., The Ramsey method in high-precision mass spectrometry with Penning traps: Experimental results, *Int. J. Mass Spectrom.*
549 264 (2007) 110, <https://doi.org/10.1016/j.ijms.2007.04.003>.
- 550 [19] T. Eronen, et al., Preparing isomerically pure beams of short-lived nuclei at JYFLTRAP, *Nucl. Instrum. Methods Phys. Res. B* 266 (2008)
551 4527, <https://doi.org/10.1016/j.nimb.2008.05.076>.
- 552 [20] S. Eliseev, et al., A phase-imaging technique for cyclotron-frequency measurements, *Appl. Phys. B* 114 (2014) 107. doi:10.1007/
553 s00340-013-5621-0.
- 554 [21] P. Dupré, et al., High-resolution mass separation by phase splitting and fast centering of ion motion in a Penning trap, *Int. J. Mass Spectrom.*
555 379 (2015) 33, <https://doi.org/10.1016/j.ijms.2014.12.007>.
- 556 [22] D. Nesterenko, et al., Phase-Imaging Ion-Cyclotron-Resonance technique at the JYFLTRAP double Penning trap mass spectrometer, *Eur.*
557 *Phys. J. A* 54 (2018) 154, <https://doi.org/10.1140/epja/i2018-12589-y>.
- 558 [23] S. V. Gorp, PhD Thesis, KU Leuven.
- 559 [24] T. Yamaguchi, et al., Masses of exotic nuclei, *Prog. in Part. and Nucl. Phys.* <https://doi.org/10.1016/j.pnpnp.2021.103882>.
- 560 [25] V. Manea, et al., First glimpse of the N=82 shell closure below Z=50 from masses of neutron-rich cadmium isotopes and isomers, *Phys. Rev.*
561 *Lett.* 124 (2020) 092502, <https://doi.org/10.1103/PhysRevLett.124.092502>.
- 562 [26] E. Leistenschneider, et al., Precision mass measurements of neutron-rich scandium isotopes refine the evolution of N=32 and N=34 shell
563 closures, *Phys. Rev. Lett.* 126 (2021) 042501, <https://doi.org/10.1103/PhysRevLett.126.042501>.
- 564 [27] A. de Roubin, et al., Nuclear deformation in the A=100 region: Comparison between new masses and mean-field predictions, *Phys. Rev. C*
565 96 (2017) 014310, <https://doi.org/10.1103/PhysRevC.96.014310>.
- 566 [28] H. Schatz, et al., Nuclear masses in astrophysics, *Int. J. Mass Spectrom.* 349 (2014) 181, <https://doi.org/10.1016/j.ijms.2013.03.016>.
- 567 [29] M. R. Mumpower, et al., The impact of individual nuclear properties on r-process nucleosynthesis, *Prog. in Part. and Nucl. Phys.* 86 (2016)
568 86, <https://doi.org/10.1016/j.pnpnp.2015.09.001>.
- 570 [30] T. Eronen, et al., High-precision QEC-value measurements for superallowed decays, *Eur. Phys. J. A* 48 (2012) 48, <https://doi.org/10.1140/epja/i2012-12048-y>.
- 571 [31] S. Eliseev, et al., Penning-trap mass spectrometry for neutrino physics, *Int. J. Mass. Spectrom.* 349 (2013) 102, <https://doi.org/10.1016/j.ijms.2013.03.010>.
- 574 [32] G. Gabrielse, et al., Open-endcap Penning traps for high precision experiments, *Int. J. Mass Spectrom.* 88 (1989) 319, [https://doi.org/10.1016/0168-1176\(89\)85027-X](https://doi.org/10.1016/0168-1176(89)85027-X).
- 576 [33] S. Eliseev, et al., Octupolar-excitation Penning-trap mass spectrometry for q-value measurement of double-electron capture in ^{164}Er , *Phys.*
577 *Rev. Lett.* 107 (2009) 152501, <https://doi.org/10.1103/PhysRevLett.107.152501>.
- 578 [34] N. Ramsey, Experiment with separated oscillatory fields and hydrogen masers, *Rev. Mod. Phys.* 62 (1990) 541, <https://doi.org/10.1103/RevModPhys.62.541>.
- 580 [35] M. Heck, PhD Thesis, University of Heidelberg.
- 581 [36] M. Rosenbusch, et al., A study of octupolar excitation for mass-selective centering in Penning traps, *Int. J. Mass Spectrom.* 314 (2012) 6–12,
582 <https://doi.org/10.1016/j.ijms.2012.01.002>.
- 583 [37] M. Rosenbusch, et al., Buffer-gas-free mass-selective ion centering in Penning traps by simultaneous dipolar excitation of magnetron motion

- 584 and quadrupolar excitation for interconversion between magnetron and cyclotron motion, *Int. J. Mass Spectrom.* 325-327 (2012) 51–57,
585 <https://doi.org/10.1016/j.ijms.2012.06.008>.
- 586 [38] M. Koenig, et al., Quadrupole excitation of stored ion motion at the true cyclotron frequency, *Int. J. Mass Spectrom.* 31 (1995) 95, [https://doi.org/10.1016/0168-1176\(95\)04146-C](https://doi.org/10.1016/0168-1176(95)04146-C).
- 587 [39] S. Eliseev, et al., Phase-Imaging Ion-Cyclotron-Resonance measurements for short-lived nuclides, *Phys. Rev. Lett.* 110 (2013) 082501, <https://doi.org/10.1103/PhysRevLett.110.082501>.
- 588 [40] R. O. the others, Precision mass measurements of neutron-rich neodymium and samarium isotopes and their role in understanding rare-earth
589 peak formation, *Phys. Rev. Lett.* 120 262702, <https://link.aps.org/doi/10.1103/PhysRevLett.120.262702>.
- 590 [41] J. Karthein, et al., Direct decay-energy measurement as a route to the neutrino mass, 7th International Conference on Trapped Charged Particles
591 and Fundamental Physics 240 61. doi:10.1007/s10751-019-1601-z.
- 592 [42] M. Gerbaux, et al., The General Purpose Ion Buncher: a radiofrequency quadrupole cooler-buncher for DESIR at SPIRAL2, in preparation.
- 593 [43] P. Shidling, et al., The TAMUTRAP facility: A Penning trap facility at Texas A&M University for weak interaction studies, *Int. J. Mass
594 Spectrom.* 468 (2021) 116636, <https://doi.org/10.1016/j.ijms.2021.116636>.
- 595 [44] M. U. Diaz, et al., A broad-band FT-ICR Penning trap system for KATRIN, *Int. J. Mass Spectrom.* 288 (2009) 1, [https://doi.org/10.
596 1016/j.ijms.2009.07.003](https://doi.org/10.1016/j.ijms.2009.07.003).
- 597 [45] <http://www.stahl-electronics.com>.
- 598 [46] R. Kersevan, M. Ady, Recent developments of Monte-Carlo codes Molflow+ and Synrad+, 10th Int. Particle Accelerator Conf. 1327–
599 1330doi:doi:10.18429/JACoW-IPAC2019-TUPMP037.
- 600 [47] C. Jamet, et al., Beam diagnostic overview of the SPIRAL2 RNB section, *Proc. 10th European Workshop on Beam Diagnostics and Instru-
601 mentation for Particle Accelerators (DIPAC'11)* (2011) 314–316.
- 602 [48] J. Vignet, et al., The beam profile monitors for SPIRAL2, *Proceedings of DIPAC2009*<http://dx.doi.org/10.13140/2.1.4214.6569>.
- 603 [49] Australian Synchrotron redpitaya-epics driver<https://github.com/AustralianSynchrotron/redpitaya-epics>.
- 604 [50] L. Dalesio, et al., The experimental physics and industrial control system architecture: past, present and future, *Nucl. Instrum. Methods Phys.
605 Res. A* 352 (1994) 179, [https://doi.org/10.1016/0168-9002\(94\)91493-1](https://doi.org/10.1016/0168-9002(94)91493-1).
- 606 [51] E. Lécorché, et al., Overview of the GANIL Control Systems for the Different Projects Around the Facility, *Proc. of International Conference
607 on Accelerator and Large Experimental Control Systems (ICALPCS'17)*, Barcelona, Spain, 8-13 October 2017 (2018) 406–410<https://doi.org/10.18429/JACoW-ICALPCS2017-TUPHA016>.
- 608 [52] T. Eronen, Private communication.
- 609 [53] <http://www.cryogenic.co.uk>.
- 610 [54] P. Anderson, Theory of flux creep in hard superconductors, *Phys. Rev. Lett.* 9 (1962) 309, [https://doi.org/10.1103/PhysRevLett.9.
611 309](https://doi.org/10.1103/PhysRevLett.9.309).
- 612 [55] L. Brown, G. Gabrielse, Geonium theory: Physics of a single electron or ion in a Penning trap, *Rev. Mod. Phys.* 58 (1986) 233, <https://doi.org/10.1103/RevModPhys.58.233>.
- 613 [56] G. Gabrielse, Why is sideband mass spectrometry possible with ions in a Penning trap ?, *Phys. Rev. Lett.* 102 (2009) 172501, <https://doi.org/10.1103/PhysRevLett.102.172501>.
- 614 [57] <http://www.simion.com>.

Declaration of interests

The authors declare that they have no known competing financial interests or personal relationships that could have appeared to influence the work reported in this paper.

The authors declare the following financial interests/personal relationships which may be considered as potential competing interests:

